Molecular Therapy
Nucleic Acids
Original Article

CircITSN1/EIF4A3/Itsn1 axis mediates postoperative cognitive dysfunction in aged mice: A novel mechanism and therapeutic target

Changteng Zhang,[1,2,8] Xiaoyu Zhu,[1,2,8] Rui Gao,[1,2] Hai Chen,[3] Caiyi Yan,[1,2] Wangyang Liu,[1,2] Lina Yang,[4] Xianzheng Zeng,[5] Haoran Yang,[6] Jin Liu,[1,2] Qi Li,[1,2] Daqing Ma,[7] Tao Zhu,[1,2] and Chan Chen[1,2]

[1]Department of Anesthesiology, West China Hospital, Sichuan University, Chengdu 610041, Sichuan, China; [2]Laboratory of Anesthesia and Critical Care Medicine, National-Local Joint Engineering Research Centre of Translational Medicine of Anesthesiology, West China Hospital, Sichuan University, Chengdu 610041, Sichuan, China; [3]Department of Respiratory and Critical Care Medicine, Targeted Tracer Research and Development Laboratory, West China Hospital 610041, Sichuan University, Chengdu, Sichuan, China; [4]Department of Anesthesiology, Sichuan Provincial People's Hospital, University of Electronic Science and Technology of China, Chengdu 610072, Sichuan, China; [5]Department of Pain Management, West China Hospital, Sichuan University, Chengdu 610041, Sichuan, China; [6]Shool of Educational Science, Chongqing Normal University, Chongqing 401331, China; [7]Division of Anaesthetics, Pain Medicine and Intensive Care, Department of Surgery and Cancer, Faculty of Medicine, Imperial College London, Chelsea and Westminster Hospital, London SW72AZ, UK

Circular RNAs (circRNAs) are stable noncoding RNAs that play a crucial role in neurodegenerative diseases, and they have been implicated in the pathogenesis of postoperative cognitive dysfunction (POCD). However, their underlying molecular mechanisms in POCD remain poorly understood. This study identified hsa_circRNA_061570 as significantly upregulated in plasma after anesthesia/surgery using high-throughput circRNA microarray screening, correlating with cognitive decline. Its murine homolog, circITSN1, was further investigated using shRNA-mediated knockdown in the hippocampus. Behavioral tests (open field, Y maze, and fear conditioning) revealed that circITSN1 suppression improved spatial and contextual memory without affecting motor function. Neuronal damage analysis via Golgi staining demonstrated that circITSN1 knockdown alleviated synaptic and dendritic spine impairments. Mechanistically, circITSN1 directly bound to RNA-binding protein EIF4A3, stabilizing *Itsn1* mRNA and activating the JNK inflammatory pathway, thereby increasing pro-inflammatory cytokines. Spatial co-localization of circITSN1 with neuronal markers and EIF4A3 underscored its neuron-specific regulatory role. These findings establish circITSN1 as a critical mediator of neuroinflammation through JNK pathway activation, positioning it as both a diagnostic biomarker and a promising therapeutic target for POCD intervention. The study bridges circRNA biology with neurocognitive pathology, offering novel insights into post-surgical cognitive impairment mechanisms.

INTRODUCTION

Postoperative cognitive dysfunction (POCD) is a common postoperative severe neurological complication in elderly surgical individuals, with a reported incidence of up to 54%.[1] It is characterized by a decline in cognitive functions, including memory, attention, information processing, and cognitive flexibility.[2] Additionally, POCD extends the duration of patients' hospital stays and elevates their financial burdens.[3,4] Most importantly, the impact of POCD on the cognitive function of geriatric patients lasts for several years and may increase the risk of multiple neurodegenerative diseases, such as Alzheimer's disease (AD).[5,6] However, the pathophysiologic processes of POCD and possible targets for therapeutic intervention remain unknown.

Surgical trauma and stress lead to cell death, followed by the release of a variety of damage-associated molecular patterns (DAMPs), which are recognized by pattern recognition receptors to induce sterile neuroinflammation, and the inflammatory response appears to be a key factor in the development of POCD.[7–9] Circular RNAs (circRNAs), as one of the DAMPs, may be triggered by surgical trauma to release them in large quantities, resulting in neuroinflammation.[10,11] Moreover, circRNAs, noncoding RNAs characterized by covalently linked 5′ and 3' ends, are reportedly involved in multiple neurodegenerative diseases, such as Parkinson's disease and AD.[12,13] Since circRNAs are enriched in the brain, they can regulate various physiological and pathological processes in nerve cells and mediate the occurrence and development of nervous system diseases.[12] Of note, compared with traditional linear RNAs, circRNAs are more stable in the blood or tissues, indicating that circRNAs have excellent potential as biomarkers for diagnosing and treating the disease.[14,15] In recent years,

Received 9 February 2025; accepted 30 April 2025;
https://doi.org/10.1016/j.omtn.2025.102555.

[8]These authors contributed equally

Correspondence: Tao Zhu, Department of Anesthesiology, West China Hospital, Sichuan University, Chengdu 610041, Sichuan, China.
E-mail: xwtao.zhu@foxmail.com
Correspondence: Chan Chen, Department of Anesthesiology, West China Hospital, Sichuan University, Chengdu 610041, Sichuan, China.
E-mail: chenchan@scu.edu.cn

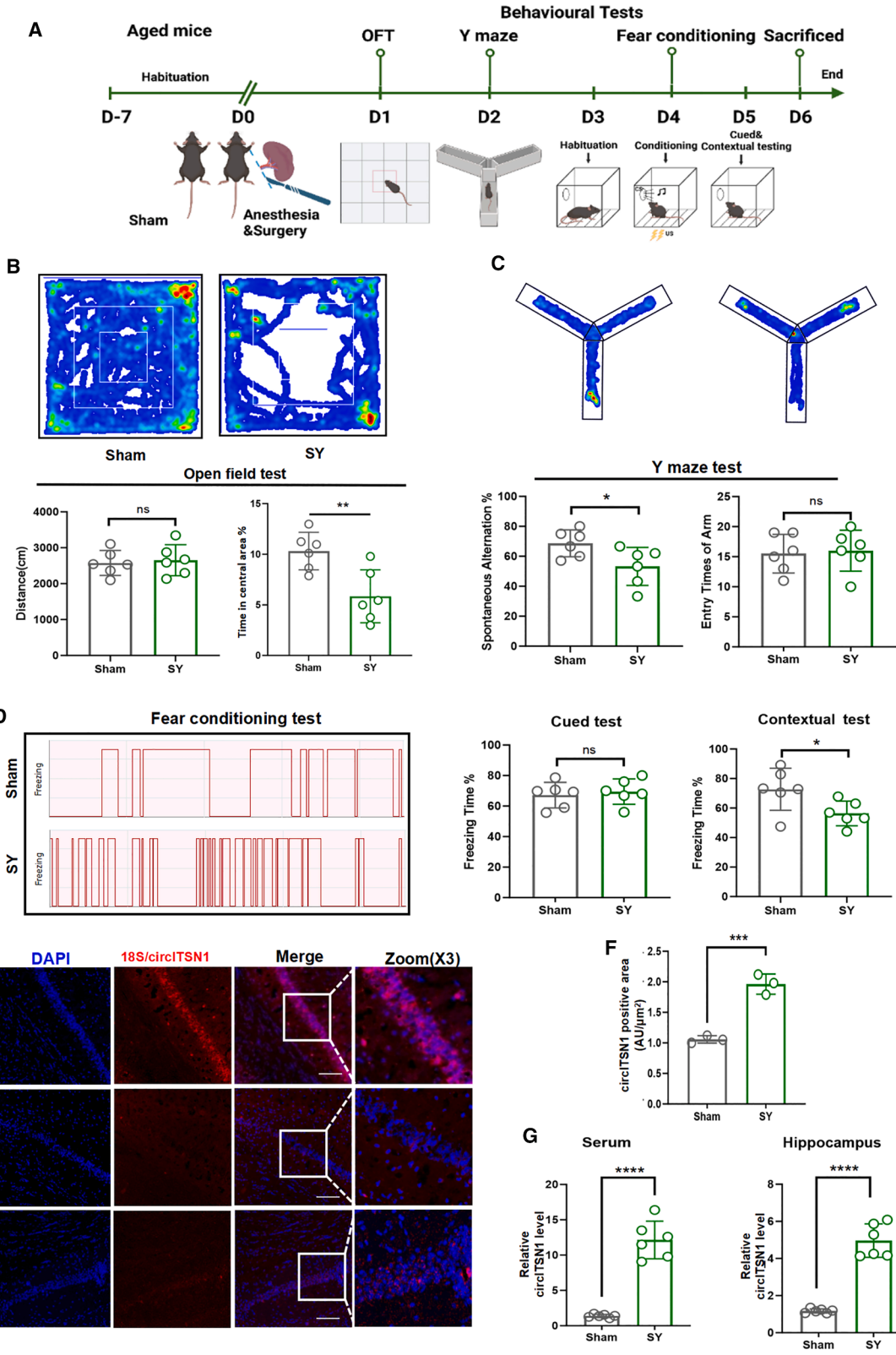

(legend on next page)

an increasing number of studies have proven that circRNAs participate in the pathological processes of POCD.[16,17] For example, Wei et al. analyzed the differential expression profile of circRNAs in the hippocampus of 12-month-old mice and reported that mmu_circRNA_26701 and its parent gene HOMER1 were increased in the glutamate synapse.[18] However, few studies have clarified the specific functions and mechanisms of circRNAs in the pathogenesis of POCD.

In our previous study, we conducted a combined microarray analysis on elderly surgical patients with and without POCD, initially identifying the upregulated hsa_circRNA_00061570 (renamed circITSN1) in the plasma of elderly POCD patients. In the current study, we further validated the expression of circITSN1 and explored its downstream mechanisms using the mouse model. The primary aim of this study is to investigate the role and underlying mechanisms of circITSN1 in the development of POCD. We hypothesized that circITSN1 interacts with the RNA-binding protein EIF4A3 to stabilize *Itsn1* mRNA, thereby activating the JNK inflammatory signaling pathway. This activation leads to synaptic and dendritic spine damage, resulting in cognitive impairment. By elucidating the circITSN1/EIF4A3/Itsn1 axis, this study seeks to identify potential biomarkers and therapeutic targets for the prevention and treatment of POCD.

RESULTS

Cognitive decline occurred in aged mice after unilateral nephrectomy

Following the test paradigm (Figure 1A), there was no significant difference in the moving distance of mice between the sham group and the surgery (SY) group, while the SY group spent less time in the center area (Figure 1B). This suggested that surgery did not impact motor ability, but the SY group exhibited increased anxiety levels. On day 3 after surgery, spontaneous alternation was reduced in the mice of SY group compared with the sham group in the Y maze test (Figure 1C). There was no significant difference between the two groups in the freezing time of the mice at the training baseline or in the cue tone test, while significantly decreased freezing time was found in the contextual test in the SY group compared with the sham group. This indicates that the SY group mice have impaired memory of fear stimuli (Figure 1D). Thus, these results indicated that unilateral nephrectomy could cause hippocampus-dependent cognitive decline in aged mice and the successful establishment of an aged mouse model of POCD.

CircITSN1 and its parental gene *Itsn1* are highly expressed in the hippocampus of aged mice after unilateral nephrectomy

The experimental process is shown in Figure S1A. In our previous research, to investigate the potential involvement of circRNAs in POCD, the blood of non-POCD (NPOCD) group (including 59 patients) and POCD group (including 39 patients) were collected, and serum samples were analyzed for circRNA expression profiles using a high-throughput circRNA microarray. A total of 210 circRNAs were differentially expressed between groups (133 upregulated and 77 downregulated in POCD patient serum) (Figures S1B–S1D). Among these differentially expressed circRNAs, hsa_circRNA_061570 was highly increased in the serum of POCD patients. Using circBase (http://www.circbase.org) and NCBI BLAST (https://blast.ncbi.nlm.nih.gov/Blast.cgi) to perform homologous transformation between humans and mice, circITSN1 was the murine circRNA homologous to hsa_circRNA_061570, and the sequencing matching degree was 90% (Figures S2A–S2C). To determine circITSN1 expression in aged mice after unilateral nephrectomy, we performed immunofluorescence staining of circITSN1 through the circRNA probe while the mice were sacrificed on day 6 post-surgery. We found a significant increase in circITSN1 levels in the SY group compared with those in the sham group after surgery (Figures 1E and 1F). In addition, we performed real-time quantitative PCR (RT-qPCR) to measure circITSN1 expression in the hippocampus and serum of aged mice and found a significant increase in circITSN1 levels in the SY group compared with those in the sham group (Figure 1G). Since circITSN1 was generated from the *Itsn1* gene, we also investigated the expression of *Itsn1*. Western blotting showed increased ITSN1 protein in the hippocampus in the SY group compared with the sham group (Figures 2A and 2B). In addition, we performed dual immunofluorescence staining of ITSN1 combined with antibodies against different cell markers for neurons (MAP2), astrocytes (GFAP), and microglia (IBA1). The increased ITSN1 expression was primarily located in MAP2-marked hippocampal neurons (Figures 2C and 2D) rather than in IBA1-marked microglia and GFAP-marked astrocytes (Figures 2E–2H). These results showed that circITSN1 and its parental gene, *Itsn1*, may play critical roles in the occurrence of POCD in aged mice.

Mice subjected to unilateral nephrectomy presented activation of JNK pathway, inflammatory cytokine release, and impaired hippocampal dendritic spines

JNK signaling, as an intracellular entity with a strong response to different stressors in the brain, is associated with neuronal plasticity and dendrite formation.[19,20] To analyze the activation of the JNK inflammatory pathway in POCD, we investigated the phosphorylation

Figure 1. Anesthesia and unilateral nephrectomy led to cognitive impairment in aged mice

(A) Schematic outline of the animal experimental design of the POCD mouse model and behavioral test. (B) Representative chart of the open field test of the sham and SY groups. Quantification of total distance and time in the central area in the open field test. (C) Representative chart of the Y-maze test of the sham and SY groups is shown. Quantification of spontaneous alteration rate and total arm entry times in the Y-maze test. (D) Percentage of freezing time in the fear conditioning cued and contextual test experiment. The percentage of freezing time was defined as the ratio of freezing time to the total time of the test process. (E) FISH analysis showing the position and expression level of circITSN1 in the CA1 region of the hippocampus in both the sham and SY groups. Scale bars, 100 μm. (F) Quantitative analysis of the relative intensity of circITSN1 in the CA1 region of the hippocampus in both the sham and SY groups ($n = 3$). (G) Expression of circITSN1 in the hippocampus and serum was measured by RT-qPCR ($n = 6$). Representative chart of test freezing time. All data are presented as the mean ± SEM; $^{*}p < 0.05$, $^{**}p < 0.01$, $^{***}p < 0.001$, and $^{****}p < 0.0001$.

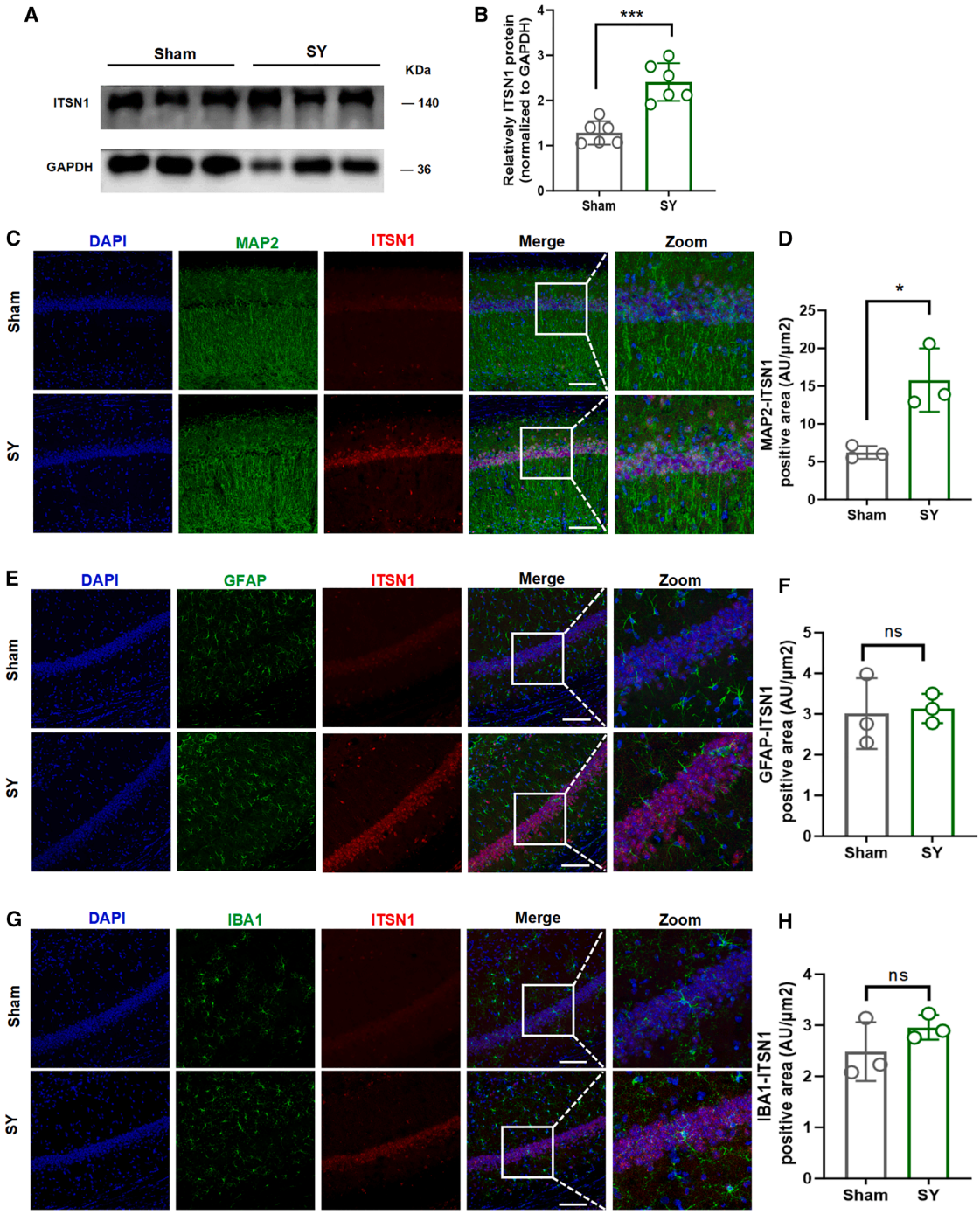

Figure 2. ITSN1 was increased in the hippocampus of the POCD mouse model

(A and B) Western blots of ITSN1 and quantitative analysis of relative band intensity (n = 6). (C and D) Immunofluorescence of ITSN1 and MAP2 from aged WT mice hippocampus samples after surgery compared to the sham group. ITSN1 (red) indicated the ITSN1 expression level and MAP2 (green) was used to stain neurons (n = 3). (E–H) Immunofluorescence of ITSN1 and GFAP/IBA1 from aged WT mice hippocampus samples after surgery compared to the sham group. ITSN1 (red) indicated the ITSN1 expression level and GFAP (green) was used to stain astroglia in (E). IBA1 (green) for microglia in (G). Quantitative analysis of GFAP-ITSN1 and IBA1-ITSN1 positive area in (F) and (H). Pictures were obtained by fluorescence microscopy (n = 3). Scale bars, 100 μm. All data are presented as the mean ± SEM; $^{*}p < 0.05$, $^{**}p < 0.01$, $^{***}p < 0.001$, and $^{****}p < 0.0001$.

of c-Jun (P-c-Jun levels over total c-Jun levels: p-c-Jun/c-Jun) and JNK (p-JNK levels over total JNK levels: p-JNK/JNK) in the hippocampus. The results showed that the P-c-Jun/c-Jun and P-JNK/JNK ratios were significantly higher in mice in the SY group than in mice in the sham group (Figures 3A–3C), indicating significant activation of the JNK stress pathway in the aged mouse model of POCD. To further investigate the impact of JNK activation on neuroinflammation, we examined the expression of JNK-related inflammatory cytokines (mainly including interleukin [IL]-1β, IL-6, and tumor necrosis factor alpha [TNF-α]) and found significant upregulation of pro-inflammatory cytokines IL-1β, IL-6, and TNF-α (Figures 3I–3K). Under activation of neuroinflammation, hippocampal neuronal plasticity and dendrite formation were further examined. We performed Golgi staining of neuronal dendrite formation in the CA1 region, which is critical for learning and memory. We found that compared with the sham group, the spine density of the dendritic shaft and branches in CA1 pyramidal neurons of the hippocampus in the SY group were significantly decreased on day 6 after surgery (Figure 3D). In addition, the total dendritic length and number of intersections were also reduced in the SY group compared with the sham group (Figures 3E–3G). Because dendritic spines are essential targets of synaptic input, we further tested the expression of the neuronal synaptic plasticity-related proteins postsynaptic density 95 (PSD95) and synaptophysin (SYN). The expressions of PSD95 and SYN in the hippocampus in the SY group were significantly lower than that in the sham group (Figures 3H, 3L, and 3M). Taken together, these results showed that the activation of the JNK pathway may be involved in dendritic spine injury and lead to the occurrence and development of POCD.

CircITSN1 knockdown improved hippocampus-dependent memory by reducing ITSN1 expression, pro-inflammatory cytokine release, and dendritic spine injury

To determine the function of circITSN1, adeno-associated virus (AAV) circITSN1 (shcircITSN1) and the negative control AAV (conAAV) were microinjected into the bilateral hippocampus of aged mice 21 days before surgery to knockdown the expression of circITSN1 (Figures 4A–4E). Compared with the SY-conAAV group, the mice treated with SY-shcircITSN1 had significantly longer freezing times in the contextual test of fear conditioning and increased spontaneous alternation percentages in the Y maze test after unilateral nephrectomy, suggesting the involvement of circITSN1 in the development of POCD (Figures 4F–4J). Since circITSN1 is generated from the *Itsn1* gene, we investigated whether circITSN1 affects its expression. The results showed a significant decrease in the protein level of ITSN1 after the knockdown of circITSN1(Figure 4K). Based on previous research on the potential regulation roles of circRNAs,[21] we hypothesized that circITSN1 may affect the protein level of ITSN1 by regulating mRNA translation and targeting mRNA stability. ITSN1 has been reported to be the key molecule that regulates synaptic plasticity in the hippocampus and can activate the JNK pathway.[22,23] Then, we performed western blotting to examine the activation profile of the JNK pathway and found that compared with the sham-conAAV group, the P-c-Jun/c-Jun and P-JNK/JNK ratios in the hippocampus were significantly reduced in the mice of the SY-conAAV group. In contrast, the ratios were increased in the SY-shcircITSN1 group (Figures S3A and S3B). Moreover, the knockdown of circITSN1 led to significant downregulation of pro-inflammatory cytokines IL-1β, IL-6, and TNF-α in the hippocampus of surgical mice (Figure 4L). The morphology of the hippocampal and CA1 neurons determined via Golgi staining is shown in Figure S4A. Sholl analysis was used to assess dendritic branching. The dendritic intersections from the soma were significantly decreased in the SY-conAAV group (Figure S4B). Similarly, the total dendritic length was reduced in the SY-conAAV group (Figure S4C). Consistent with the aforementioned results, the spine density declined in the SY-conAAV group (Figures S4D and S4E). Moreover, the number of dendritic intersections, total dendritic length, and spine density were greater in the SY-shcircITSN1 group compared with the SY-conAAV group (Figures S4B–S4E). Compared with those in the sham-conAAV group, the expressions of PSD95 and SYN in the hippocampus were significantly lower in the SY-conAAV group. In contrast, their expressions were increased in the SY-shcircITSN1 group (Figure S4F). These results showed that circITSN1 could activate the expression of its parent gene *Itsn1* and cause dendritic spine injury in the aged mouse model of POCD.

Itsn1, the parent gene of circITSN1, promoted dendritic spine injury in the POCD model by activating the JNK pathway and pro-inflammatory cytokines

To further determine the roles of *Itsn1* in the hippocampus of aged mice after unilateral nephrectomy, we injected 0.5 μL of AAV itsn1 (shITSN1) and the conAAV into the bilateral hippocampus of aged mice 21 days before surgery to knock down the expression of *Itsn1* (Figures 5A–5D). Then, we found that compared with those in the sham-conAAV group, the mice in the SY-conAAV group presented significantly shorter contextual freezing times and a decreased spontaneous alternation percentage after surgery, while the contextual freezing time was increased and the spontaneous alternation percentage was increased in the SY-shITSN1 group, indicating the function of ITSN1 in the development of POCD (Figures 5E–5H). Meanwhile, compared with those in the sham-conAAV group, the expressions of PSD95 and SYN were significantly lower in the hippocampus of the SY-conAAV group, while their expressions were increased in the SY-shITSN1 group (Figures S5F and S5G). As reported, the JNK pathway could be activated by ITSN1. We further examined the P-c-Jun/c-Jun and P-JNK/JNK ratios in the hippocampus by western blotting. The results showed that the P-c-Jun/c-Jun and P-JNK/JNK ratios in the hippocampus were significantly increased in the mice in the SY-conAAV group, while the ratios were decreased in the mice in the SY-shITSN1 group (Figures S3C and S3D). Similarly, the knockdown of ITSN1 also significantly downregulated the expressions of the JNK-proinflammatory cytokines IL-1β, IL-6, and TNF-α in the hippocampus of surgical mice (Figures 5I–5K). Additionally, compared with that in the sham-conAAV group, the total dendritic length was reduced in the SY-conAAV group (Figures S5A–S5C), while the spine density also

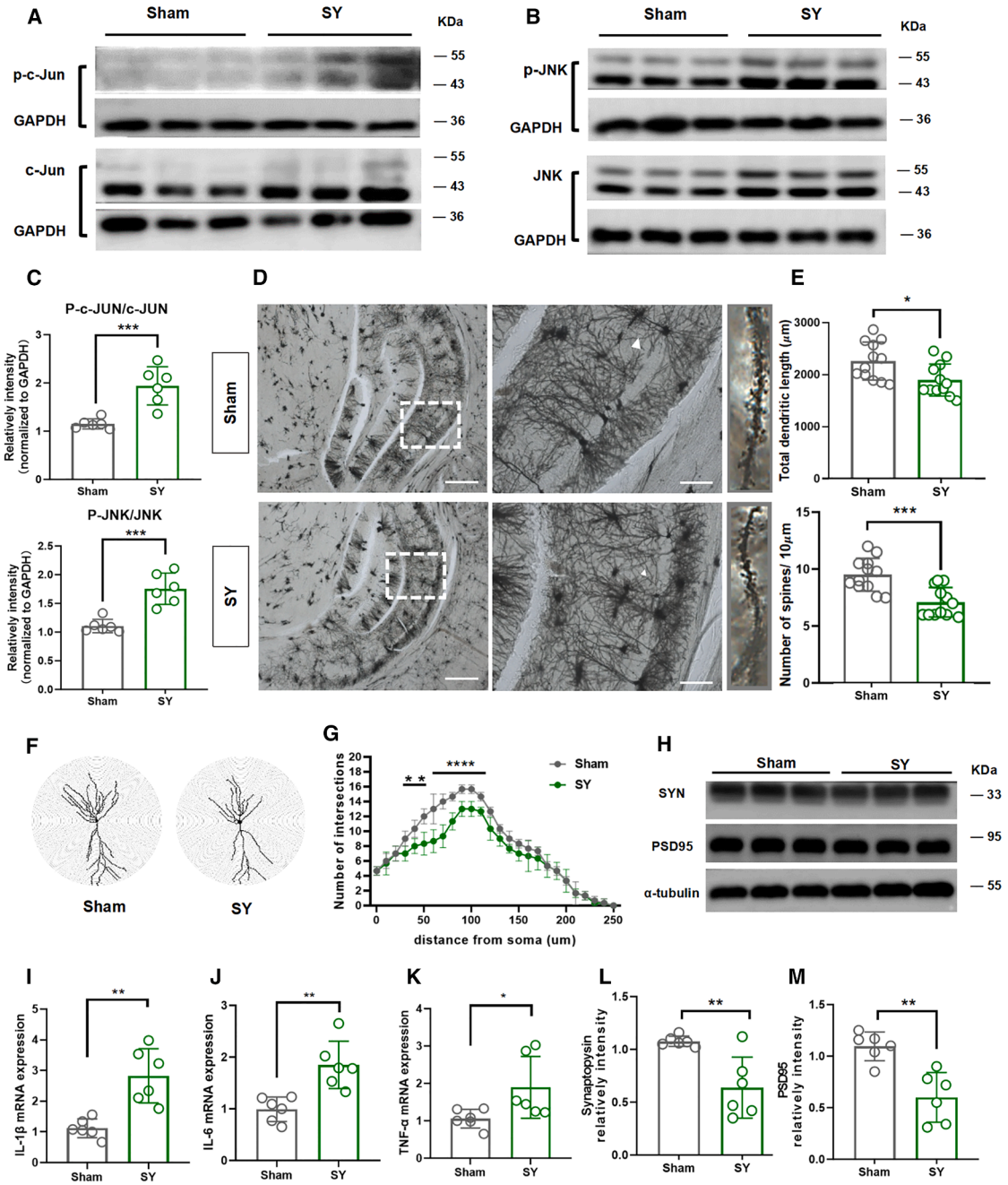

Figure 3. Anesthesia and unilateral nephrectomy led to activation of the JNK pathway and impaired hippocampal dendritic spines in aged mice

(A and B) Western blots of hippocampal tissue show the protein levels of P-c-Jun, c-Jun, P-JNK, JNK, and GAPDH in the sham and SY groups. (C) Quantitative analysis of the relative band intensity of the P-c-Jun/c-Jun and P-JNK/JNK ratios is shown ($n = 6$). (D) Golgi staining of the whole hippocampus, CA1 region, and dendritic spine. Scale bars, 500 μm and 100 μm. (E) Quantitative analysis of total dendritic length and synaptic spine density ($n = 12$). (F and G) Sholl analysis and quantitative analysis of the number of intersections. (H) Western blotting showed the protein levels of PSD95 and SYN in the hippocampus of both the sham and SY groups. (I–K) Changes in expression levels of pro-inflammatory cytokines IL-1β, IL-6, and TNF-α in the hippocampus of surgical aged mice or sham group ($n = 6$). (L and M) Quantitative analysis of the relative band intensity of PSD95 and SYN is shown ($n = 6$). All data are presented as the mean ± SEM; $^{*}p < 0.05$, $^{**}p < 0.01$, $^{***}p < 0.001$, and $^{****}p < 0.0001$.

declined in the SY-conAAV group (Figures S5D and S5E). Moreover, the number of dendritic intersections, total dendritic length, spine density, and spine density all increased in the SY-shITSN1 group compared with the SY-conAAV group (Figures S5A–S5E). These results showed that ITSN1 could activate JNK and mediate dendritic spine injury in the POCD model.

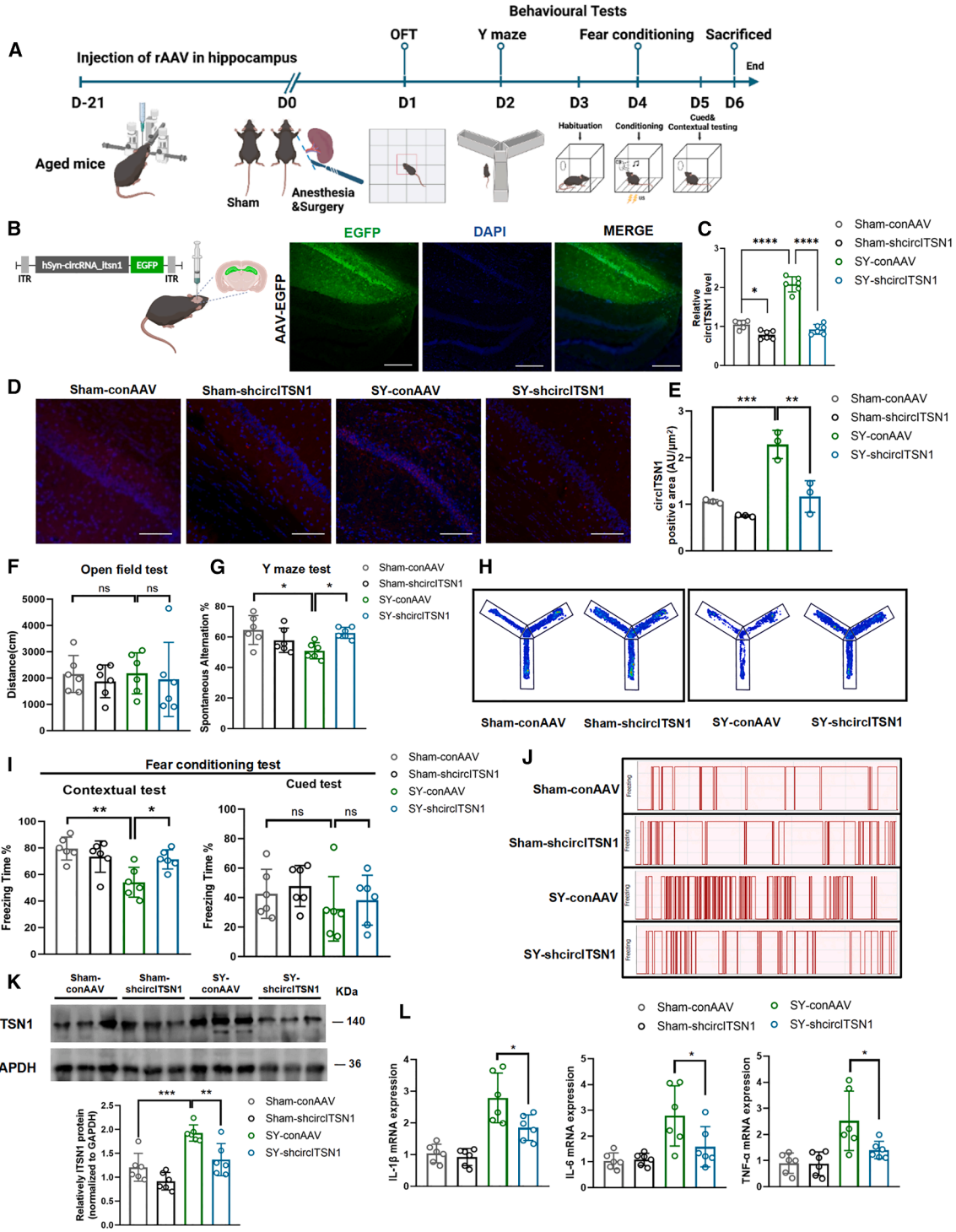

Figure 4. CircITSN1 knockdown in the hippocampus improved POCD in aged mice

(A) Schematic outline of the animal experimental design of microinjection of AAV circITSN1 and negative AAV in the hippocampus. (B) Diagrammatic drawing showing microinjection of AAV circITSN1 (shcircITSN1) and the negative control AAV (con AAV) into the bilateral hippocampus of aged mice 21 days before surgery. EGFP (green) expression levels indicated that microinjection of AAV successfully infected CA1 region neurons, as confirmed by fluorescence microscopy. Scale bars, 250 μm. (C) Expression of circITSN1 in the hippocampus after microinjection of AAV was measured by RT-qPCR ($n = 6$). (D) FISH analysis showed the expression level of circITSN1 in four groups of mice. Scale bars, 100 μm. (E) Quantitative analysis of the circITSN1 positive area ($n = 3$). (F) Quantification of total distance traveled in the open field test ($n = 6$). (G)

(legend continued on next page)

EIF4A3 was recruited by circITSN1 to stabilize *Itsn1* mRNA *in vivo* and *in vitro*

According to the prediction of CircInteractome (https://circinteractome.nia.nih.gov/), hsa_circRNA_061570 could bind with protein EIF4A3, indicating that hsa_circRNA_061570 has protein-binding capacity (Figures S6A–S6C). circITSN1 is the murine circRNA homologous to hsa_circRNA_061570, and the degree of sequencing matching was 90%. Thus, we speculated that circITSN1 might also bind to EIF4A3 (Figure 6A). EIF4A3 is an RNA-binding protein that plays a vital role in monitoring mRNA quality and initiating translation, while circITSN1 might work together with it to promote POCD occurrence. Thus, we detected the expression of EIF4A3 in the four groups with knockdown of circITSN1 expression. The western blot results showed the upregulation of EIF4A3 in the SY group compared with the sham group (Figures 6B and 6C). The abnormal expression of EIF4A3 implied that it is essential in POCD. Then, we investigated the role of EIF4A3 both mechanically and functionally. RNA immunoprecipitation (RIP) and RNA pull-down assays were performed to verify that circITSN1 could bind to EIF4A3 specifically (Figures 6F–6H). In the SY-conAAV group, the *in-situ* hybridization results showed the co-localization of circITSN1 and EIF4A3 by confocal microscopy (Figures 6D and 6E). In addition, we overexpressed circITSN1 in HT-22 cells, a mouse hippocampal cell line, and performed *in situ* hybridization, which revealed the co-localization of circITSN1 and EIF4A3 (Figures 7A and 7B). An RIP assay also confirmed that circITSN1 could bind to EIF4A3 specifically *in vitro* (Figure 7E). After circRNA was overexpressed in HT22 cells, there was no significant change in the mRNA levels of *Itsn1* compared with those in the control group (Figure 7D). However, a significant increase in ITSN1 protein level in the LV-circITSN1 group was confirmed by western blot analysis, indicating that circITSN1 mainly affects the process of protein translation. (Figure 7C). We are trying to uncover the truth behind the changes in ITSN1 protein levels despite the lack of significant differences in *Itsn1* mRNA levels. EIF4A3 has been reported to bind circRNAs to regulate mRNA stability.[24] By performing an RIP assay, we confirmed the essential binding between *Itsn1* mRNA and EIF4A3 (Figure 7F). Then, we investigated the stability of *Itsn1* mRNA in HT-22 cells subjected to actinomycin D after overexpressing circITSN1 and inhibiting the expression of EIF4A3. We found that overexpressing circITSN1 could significantly increase the stability of *Itsn1* mRNA, while EIF4A3 siRNA could significantly inhibit the mRNA stability of *Itsn1* (Figure 7G). In summary, the results demonstrated that circITSN1 recruited EIF4A3 to increase ITSN1 expression by enhancing the stability of *Itsn1* mRNA.

DISCUSSION

Our study demonstrated that circITSN1 was upregulated in the hippocampal tissue and serum of aged mice following unilateral nephrectomy under anesthesia. circITSN1 exacerbated dendritic spine injury and cognitive decline, which were reversed with circITSN1 knockdown. Mechanistically, circITSN1 interacted with EIF4A3 and regulated the expression of the parental gene *Itsn1*, activating the JNK pathway. Therefore, our study was the first to demonstrate the critical role of circITSN1 and its host gene *Itsn1* in POCD development in aged mice.

Increasing evidence suggests that the abnormal expression of circRNAs is associated with many pathophysiological processes and plays a vital role in the development of neurodegenerative diseases, including AD, Parkinson's disease, and other disease conditions.[13,25,26] hsa_circRNA_061570 was significantly increased in the postoperative serum of POCD patients. HOMER1 and its transcript mmu_circRNA_26701 were reported to be specifically enriched in glutamate synapses in aged mice with postoperative delirium.[18] To date, the specific functional mechanism of circRNAs in POCD has not been clarified, even though researchers have performed many screening and prediction studies on patients' biological samples or animal models of POCD.[16,27] Our previous study successfully screened 210 differentially expressed circRNAs, with 133 upregulated and 77 downregulated circRNAs, in the serum of POCD patients and non-POCD patients.[28] Based on the screening process, in this study, we selected circITSN1, which is homologous to hsa_circRNA_061570 and whose parental gene *Itsn1* plays a crucial role in regulating synaptic plasticity and neurodegenerative disease.[29]

Although the potential role of circRNAs in neurodegenerative diseases has been widely reported, their downstream regulatory mechanism is still largely unclear.[30] In recent studies, circRNAs were reported to regulate target mRNAs positively or negatively.[31] Qian and colleagues recently demonstrated that increased expression of circUBE3B targeted miR-326, which negatively regulated the expression of MYD88, leading to sevoflurane-induced cell apoptosis and postoperative cognitive decline.[32] circCwc27 was reported to act as a critical player in the development of AD, in which it directly bound to purine-rich element-binding protein A (Pur-α), and suppressed Pur-α recruitment to the promoters of a cluster of AD genes, inducing Aβ deposition and cognitive decline.[33] Our study found that circITSN1 acted on EIF4A3, as shown by a series of experimental measurements. EIF4A3 is an essential component of the exon junction complex and plays a critical role in mRNA splicing, localization, transportation, and translation.[34,35] For example, the long noncoding RNA *Casc11* promoted hepatocellular carcinoma progression by recruiting EIF4A3 to stabilize *E2f1* mRNA and enhance its expression.[36] In addition, EIF4A3 was also recruited by hsa_circ_0068631 to increase *C-myc* mRNA stability in breast cancer.[24] Accordingly, we speculated that the combination of circITSN1

Quantification of spontaneous alteration rate in the Y-maze test ($n = 6$). (H) Representative chart of the Y-maze test. (I) Percentage of freezing time in the fear conditioning contextual and cued test experiment. The percentage of freezing time was defined as the ratio of freezing time to the total time of the test process ($n = 6$). (J) Representative chart of the fear conditioning contextual test. (K) Western blots of hippocampal tissue and quantitative analysis of relative band intensity showed the protein level of ITSN1 in different groups ($n = 6$). (L) Changes in expression levels of pro-inflammatory cytokines IL-1β, IL-6, and TNF-α in the hippocampus of mice after circITSN1 knockdown ($n = 6$). All data are presented as the mean ± SEM; $^{*}p < 0.05$, $^{**}p < 0.01$, $^{***}p < 0.001$, and $^{****}p < 0.0001$.

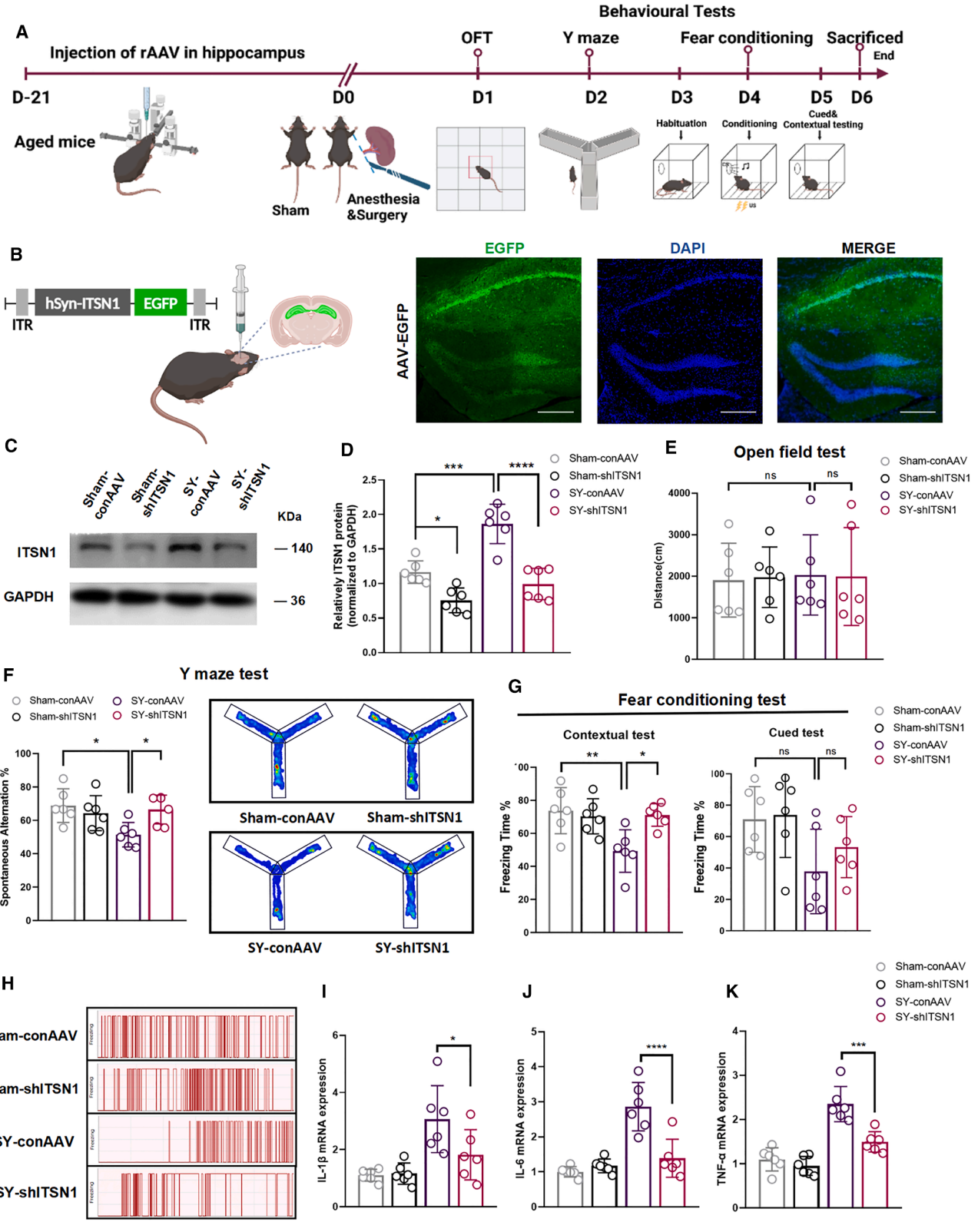

(legend on next page)

and EIF4A3 might affect the mRNA stability of *Itsn1*. This finding was verified in our *in vitro* experiments through the actinomycin D assay, and we found that overexpressing circITSN1 in HT-22 cells increased the mRNA stability of *Itsn1*.

Moreover, our study also extended the research on the downstream circITSN1/*Itsn1* regulatory associations. ITSN1, a member of the ITSN family, is an evolutionarily highly conserved protein with multiple domains and is mainly involved in the regulation of cellular endocytosis and exocytosis, as well as synaptic conduction and related signaling pathway transmission.[37–39] ITSN1 plays a critical role in neurodegenerative diseases and cognitive impairment-related diseases, such as Parkinson's disease and AD.[40,41] Synaptic plasticity dysfunction and dendritic spine injury have been reported in POCD patients, while whether ITSN1 mediates synaptic damage in POCD patients has not yet been reported.[42,43] In the present study, we found an improvement in the postoperative cognitive level and less impairment in synaptic plasticity after inhibiting *Itsn1* expression and confirmed the critical role of *Itsn1* in POCD. A previous study showed that ITSN1 enhanced huntingtin protein aggregation and neurodegeneration by activating JNK. The JNK pathway is an intracellular pathway that strongly responds to different stressors and plays a vital role in central nervous system maintenance and development.[44] JNK has been reported to control synaptic function and neuronal plasticity, mediate neuroinflammation, and influence memory formation.[45–48] Recently, activation of the JNK pathway has also been widely reported in POCD.[49] Notably, Rossato and colleagues reported the critical roles of JNK and c-Jun in responding to stress stimuli and contributing to hippocampal synaptic plasticity.[50] Moreover, JNK signaling activation induces the release of related downstream pro-inflammatory cytokines, such as IL-1β, IL-6, and TNF-α.[51] Thus, the expression of JNK/p-JNK and its downstream signals c-jun/p-c-jun in the hippocampus of aged mice detected in our study indicated the activation of JNK signaling in aged POCD mice. In contrast, the activation of JNK was alleviated after knocking down *Itsn1*, accompanied by a reduction of pro-inflammatory cytokines and improvement of dendritic spine injury in the hippocampus. In summary, we found that circITSN1 affected its parental gene *Itsn1* by recruiting EIF4A3 and further activating the JNK signaling pathway accompanied by dendritic spine injury. All these interact with each other to trigger POCD occurrence.

In summary, our study mechanistically and functionally demonstrated that circITSN1 stabilized the parental gene *Itsn1* mRNA by recruiting EIF4A3 and then activating the JNK signaling pathway, thus increasing hippocampal neuroinflammation and driving POCD development. Suppressing the circITSN1/EIF4A3/*Itsn1* axis may inspire new therapeutic strategies for preventing and treating POCD. In addition, unlike traditional linear RNA, circRNA has a closed ring structure that is not degraded by RNA exonucleases and is more stable and highly expressed in body fluids.[52] Therefore, circRNAs may be considered new ideal diagnostic biomarkers for POCD in the future.

MATERIALS AND METHODS

Animals and POCD mouse model

Adult male C57BL/6J mice (20–22 months old, weighing 28–35 g), purchased from Chengdu Dossy Experimental Animals Co., Ltd., were group-housed six per cage on a 12-h light/dark cycle in a temperature-controlled (25 ± 2°C) room with free access to water and food. They were allowed 7 days to adapt to our new breeding environment before the experiment. The study was approved by the Animal Care and Use Committee of West China Hospital (no. 20230526004) and followed the ARRIVE Guidelines.[53]

The mice were subjected to a unilateral nephrectomy operation under isoflurane anesthesia, as reported previously, with some modifications.[54] They were randomly assigned to the sham or SY groups. Specifically, anesthesia was induced with 3.0% isoflurane, followed by maintenance with 1.5% isoflurane carried by gases containing 30% oxygen. Each mouse was placed in the right lateral position, and a 1 cm transverse incision under the costal margin was made to remove the left kidney. At the same time, the sham group received identical treatments except without anesthesia or surgery. The entire procedure, from the induction of anesthesia to the end of surgery, lasted 2 h. A heating pad was used to maintain the body temperature between 36°C and 37°C during the surgery. Following the surgery, all the mice were allowed to recover fully before being returned to their home cages.

Behavioral test

Open field test (OFT): Mice were assessed in an open rectangular box with a bottom edge length of 50 × 50 cm and a height of 60 cm (RWD Life Science, Shenzhen, China) on day 1 after surgery or mock treatment. After being placed in the intermediate region of the box, animal behavior was recorded by a camera for 5 consecutive minutes. The bottom of the box was divided into a central region (30 × 30 cm^2) and the remaining peripheral region. The time spent

Figure 5. *Itsn1* knockdown in the hippocampus improved POCD in aged mice

(A) Schematic outline of the animal experimental design of AAV itsn1 (shitsn1) microinjection and negative control AAV in the hippocampus. (B) Diagrammatic drawing showing microinjection of AAV itsn1 and con AAV into the bilateral hippocampus of aged mice 21 days before surgery. EGFP (green) expression levels indicated that AAV infection of the CA1 region of the hippocampus was successfully confirmed by fluorescence microscopy. Scale bars, 250 μm. (C and D) Western blotting of hippocampal tissue and quantitative analysis of relative band intensity showed the protein levels of ITSN1 and GAPDH in different groups ($n = 6$). (E) Quantification of total distance traveled in the ($n = 6$). (F) Quantification of spontaneous alteration rate and representative chart in the Y-maze test ($n = 6$). (G) Percentage of freezing time in the fear conditioning contextual and cued test experiment. The percentage of freezing time was defined as the ratio of freezing time to the total time of the test process ($n = 6$). (H) Representative chart of the contextual freezing time test. (I–K) Changes in expression levels of pro-inflammatory cytokines IL-1β, IL-6, and TNF-α in the hippocampus of mice after ITSN1 knockdown ($n = 6$). All data are presented as the mean ± SEM; $^{*}p < 0.05$, $^{**}p < 0.01$, $^{***}p < 0.001$, and $^{****}p < 0.0001$.

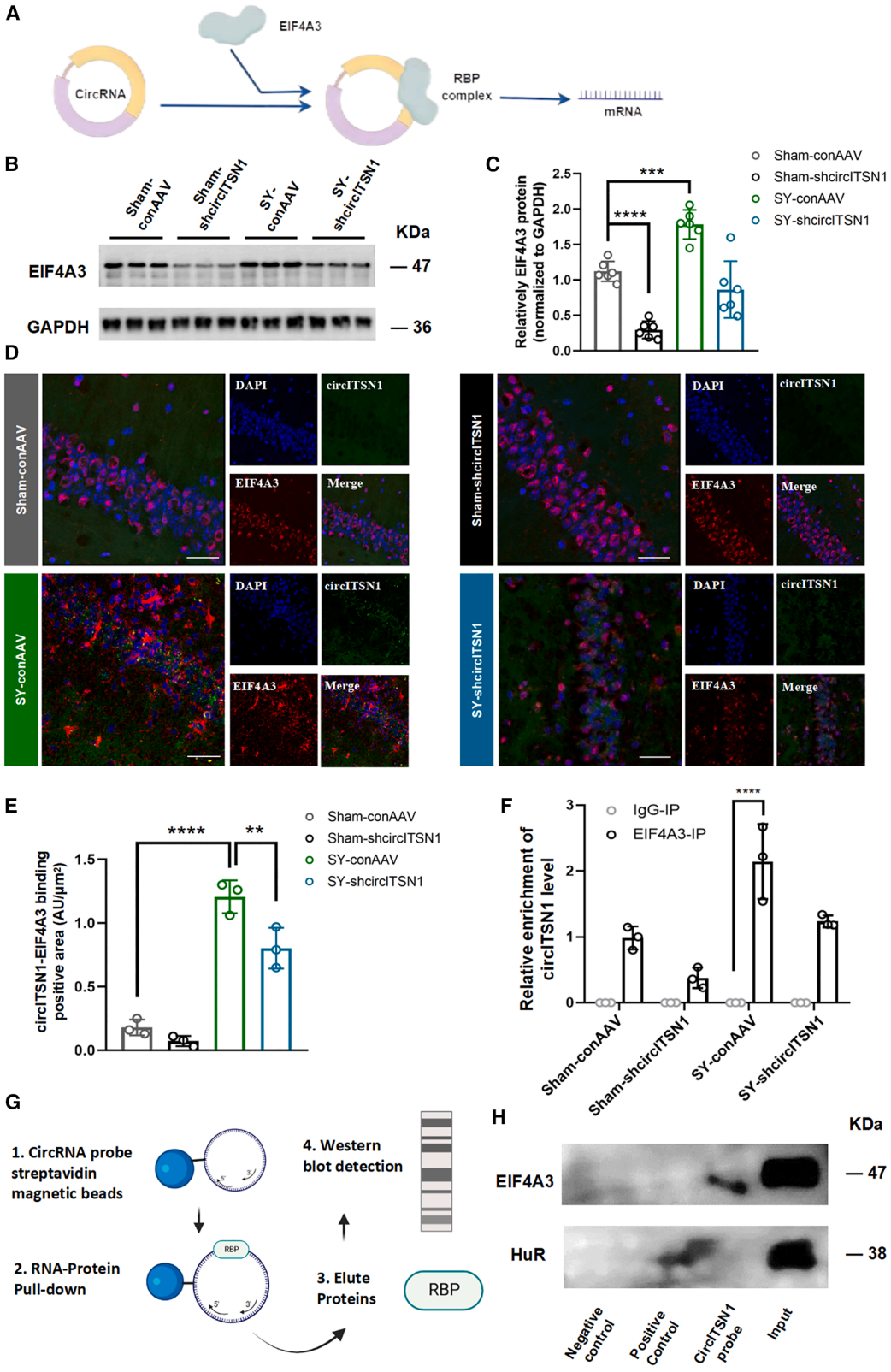

(legend on next page)

by the animal in each region, as well as the distance moved in the box, were calculated.

Y-maze test was performed as previously described on day 2 after surgery. Briefly, the Y-maze apparatus comprised three identical arms (the size of each arm: 40 cm length × 8 cm width × 15 cm height, spaced 120° apart; RWD Life Science, Shenzhen, China). Mice were placed into the maze from the fixed arm and allowed to explore freely for 8 min while tracking software recorded zone transitioning and locomotor activity (Smart 3.0 tracking software, Panlab, Kent, UK). Spontaneous alternation was defined as a mouse entering all 3 arms on consecutive choices (ABC, BCA, or CAB; but not BAB, CAC, or CBC). Spontaneous alternation was calculated using the following formula: %spontaneous alternation = (number of alternations/total arm entries −2) × 100%.

Fear conditioning test was conducted using a conditioning chamber (062814-14216, UGO BASILE S.R. L, Gemonio, Italy) and an unconditional stimulus (three periods of foot shock of 0.75 mA during 2 s). The animal motion was captured by an infrared video camera set in front of the chamber (Video Freeze; Med Associates). All groups of mice underwent habituation on day 3 after surgery and the same training session on day 4 after surgery. During the training day, mice were placed in the chamber to freely explore for 3 min, followed by 30 s of 4 Hz sound stimulation, and immediately followed by a foot electric shock (2 s, 0.75 mA). This pairing stimulus was repeated 3 times, with a 2 min interval between each repetition. On day 5 after surgery, mice were returned to the same chamber where they had been trained for contextual and cued tests. For the contextual test, mice were re-exposed to the chamber without any tones or foot shocks presented. For the cued test, mice were re-exposed just to the tones without foot shocks in a different chamber. Two investigators were blinded to the groups that recorded the "freezing behavior" analyzed by ANY-MAZE as a total lack of movement, excluding breathing and movement of vibrissae. The longer freezing time indicated that the mice had better hippocampus-dependent memory of the conditioned fear stimulus.

Specimen collection for further experiments

After the behavioral tests, hippocampal tissues and whole blood were harvested in separate cohorts under terminal anesthesia. Whole blood was collected from the right atrium and stored in RNase-free Eppendorf tubes. Then, the brain tissues were immediately removed, and the hippocampus was quickly split in ice-cold PBS, frozen in liquid nitrogen, and stored at −80°C. After the collection of the whole blood, it was left undisturbed at room temperature (RT) for approximately 30 min. Following centrifugation at 3,000 × g for 10 min at 4°C, the serum was collected. These experiments were all performed under strict RNase-free conditions, and the samples were further processed for the following experiments.

Stereotaxic surgery and intrahippocampal microinjection

The adeno-associated virus (AAV)-shcircITSN1 and control-AAV (OBiO, Co., Ltd., Shanghai, China) were diluted with PBS *in vivo* transfection reagent (Engreen, Beijing, China). AAV-shITSN1 and control-AAV (GeneChem Co., Ltd., Shanghai, China) were diluted with PBS *in vivo* transfection reagent (Engreen, Beijing, China). Bilateral intrahippocampal injection was performed using a stereotaxic apparatus (RWD Life Science, Shenzhen, China). A total of 0.5 μL of AAV-shcircITSN1 (1×10^{12}) and 0.5 μL control-AAV (1×10^{12}) were infused bilaterally in the hippocampus (0.2 μL/min) using a 33-gauge beveled NanoFil needle, a NanoFil syringe, and a MicroSyringe Pump Controller (World Precision Instruments, Sarasota, FL, USA) at the following distances from bregma: anteroposterior −2.0 mm, medio-lateral ±1.8 mm, and dorsoventral −1.7 mm. The bilateral intrahippocampal injection of AAV-shITSN1 was the same as that of AAV-shcircITSN1.

Golgi staining

For dendritic spine analysis, Golgi-stained mice were deeply anesthetized with isoflurane and sacrificed via cervical dislocation. Whole brains were processed using an FD Rapid Golgi Stain Kit (FD Neuro Technologies, USA) according to the methods provided by the manufacturer. The brains were sliced at 150 μm using a cryostat, and the sections were collected on gelatinized glass slides before dehydration in absolute ethanol, clearing in xylene, and covering slips with neutral resin (Bioworld, USA). z stack images of Golgi-stained neurons were captured using a 20× objective lens and 100× oil immersion lens via brightfield microscopy on a Zeiss confocal microscope. Sholl analysis, dendritic length, and dendritic density were analyzed using NIH ImageJ software.

Fluorescence *in situ* hybridization

The expression and cellular localization of circITSN1 in the hippocampus were detected by fluorescence *in situ* hybridization (FISH) analysis. Digoxin-labeled probe sequences for circITSN1 were synthesized for FISH analysis. The probes were designed and synthesized by Exon Biotech Inc. (Guangzhou, China), and the signals of the probes were detected by a Fluorescent *In Situ* Hybridization Kit (Exon Biotech Inc., Guangzhou, China) according to the

Figure 6. The RNA binding protein EIF4A3 interacted with circITSN1 and *Itsn1* mRNA, as verified *in vivo*

(A) Schematic representation of the interaction of the RNA binding protein EIF4A3 with circITSN1 and *Itsn1* mRNA. (B) EIF4A3 was highly expressed in the four groups with the knocked-down expression of circITSN1, as confirmed by western blots. (C) Quantitative analysis of the relative band intensity of EIF4A3 is shown ($n = 6$). (D) FISH analysis and immunofluorescence showed the positional relationship between circ_*Itsn1* and EIF4A3 in the hippocampal CA1 region of mice. Circ_*Itsn1* colocalized with EIF4A3 mainly in the SY-conAAV group, and circ_*Itsn1* was expressed at a low level in the other three groups. Scale bars, 20 μm. (E) Quantification of FISH analysis and immunofluorescence of the four groups are shown ($n = 3$). (F) RIP assay showed that EIF4A3 interacted with circITSN1 in the hippocampus of mice ($n = 3$). (G) Schematic diagram of the RNA pull-down assay. (H) RNA pull-down assay showed that EIF4A3 interacted with circITSN1 in the hippocampus of mice. All data are presented as the mean ± SEM; $^{*}p < 0.05$, $^{**}p < 0.01$, $^{***}p < 0.001$, and $^{****}p < 0.0001$.

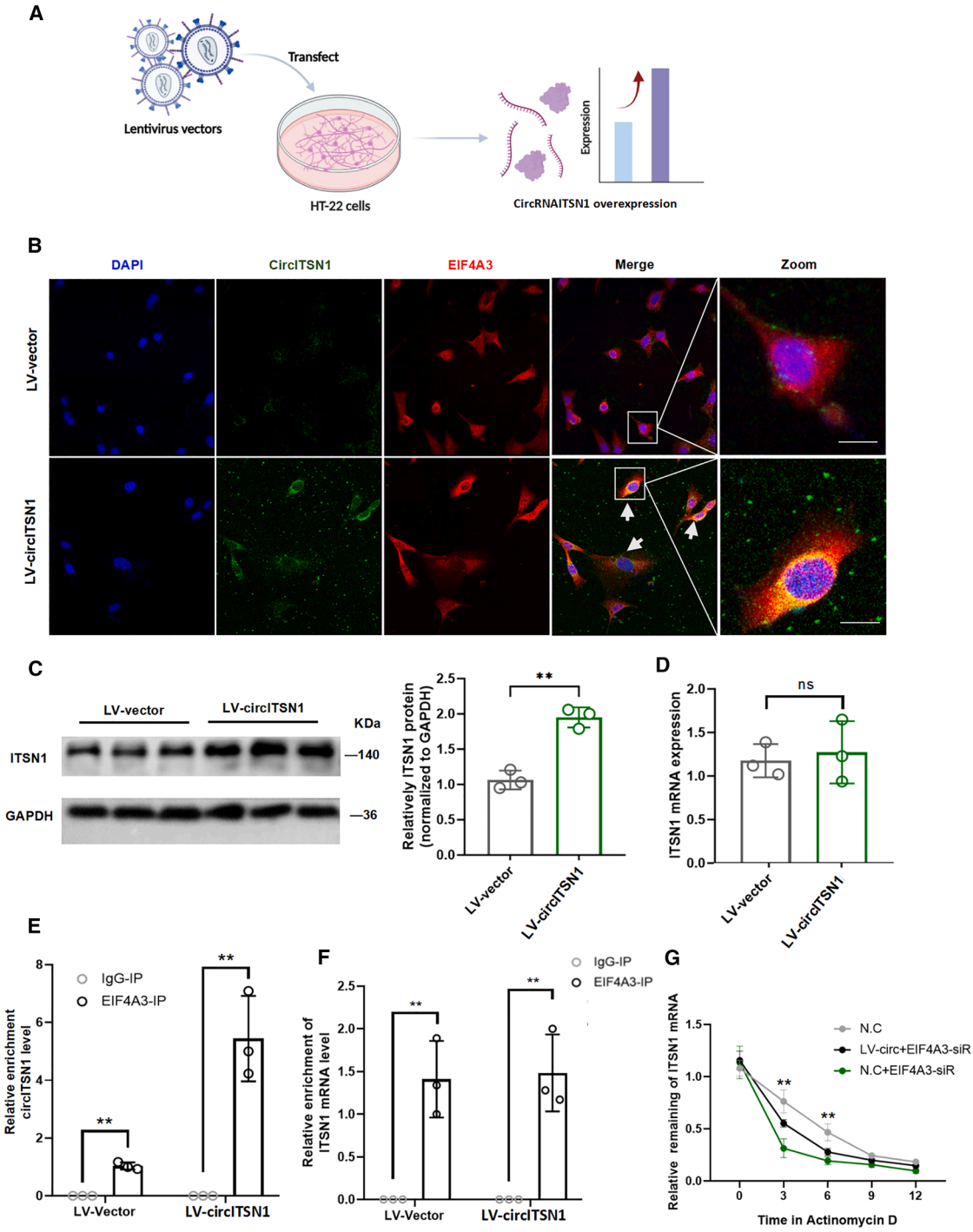

Figure 7. CircITSN1 regulates the mRNA stability of *Itsn1 in vitro*

(A) Schematic representation of overexpression of CircITSN1 in HT-22 cells. (B) FISH analysis and immunofluorescence showed that circITSN1 colocalized with EIF4A3 after overexpressing circITSN1 in HT-22 cells. Scale bars, 20 μm. (C) Western blots of ITSN1 in HT-22 cells after transfection with different lentiviruses and quantitative analysis of relative band intensity ($n = 3$). (D) Expression of *Itsn1* mRNA in HT-22 cells was measured by RT-qPCR ($n = 3$). (E and F) RIP assays showed that EIF4A3 interacted with circITSN1 and *Itsn1* mRNA in HT-22 cells ($n = 3$). (G) Overexpressing circITSN1 significantly increased the stability of *Itsn1* mRNA, while eIF4A3 siRNA significantly inhibited the mRNA stability of *Itsn1*, as confirmed by RT-qPCR at 0, 3, 6, 9, and 12 h after HT-22 cells were subjected to actinomycin D. All data are presented as the mean ± SEM; $^{*}p < 0.05$, $^{**}p < 0.01$, $^{***}p < 0.001$, and $^{****}p < 0.0001$.

manufacturer's instructions. The images were captured on a Leica SP8 Laser Scanning Confocal Microscope (Leica Microsystems, Mannheim, Germany). NIH ImageJ software was used to analyze fluorescence intensity. In brief, samples were fixed and pretreated with 4% paraformaldehyde and PBS with 0.5% Triton X-100. Then, circITSN1 Probe Mix was used to hybridize with the samples at 37°C overnight. Finally, after DAPI staining of the nuclei, the slides were imaged using a Leica laser scanning confocal microscope.

RNA immunoprecipitation

RIP was performed using an EIF4A3-specific antibody (Proteintech, cat no. 17504-1-AP, Rabbit), and an IgG antibody was used as a negative control. Immunoprecipitation was conducted using an RIP kit (Exon Biotech Inc., Guangzhou, China) according to the manufacturer's instructions. In brief, HT-22 cells were lysed in a lysis buffer containing proteinase inhibitors and RNase inhibitors. The lysate was incubated overnight with antibody-coupled magnetic beads with rotation at 4°C. Bead-antibody complexes were subsequently washed thoroughly with RIP wash buffer. RNA purification and extraction were performed using proteinase K digestion and phenol-chloroform. RNA was obtained for follow-up verification.

RNA pull-down

Lysis buffer was added to HT-22 cells, and total protein was extracted by freezing and thawing three times in liquid nitrogen. The circITSN1 probe (Exon Biotech Inc., Guangzhou, China) was added to generate a circITSN1/protein complex, which was incubated with streptavidin-complexed magnetic beads at 4°C for 6 h. The magnetic beads were extracted, and EIF4A3 protein expression was detected by western blot.

Immunofluorescence staining

In vivo, immunofluorescence staining was conducted to detect ITSN1 expression and its activated area in hippocampal tissue. The brains were removed, fixed with 4% paraformaldehyde overnight at 4°C, and dehydrated in 30% sucrose-PBS. The brain was mounted in optimal cutting temperature embedding medium, frozen, and cut coronally at a 40-μm thickness on a kryotome (Leica CM 3050S). Brain sections were stained with the following primary antibodies overnight: anti-ITSN1 monoclonal antibody (1:200, bs-18171R, Bioss), neuron marker MAP2 (1:200, ab5392, Abcam), astrocyte marker GFAP (1:200, 60190-1-Ig, Proteintech), and microglia cell marker IBA1 (1:100, 011–27991, WAKO). Primary antibodies were cleared with PBS, and brain sections were incubated with secondary antibodies at RT: Alexa Fluor 555 donkey anti-rabbit IgG (H + L) (1:500, A31572, Invitrogen), Alexa Fluor 488 donkey anti-mouse IgG (H + L) (1:500, A21202, Invitrogen), and Alexa Fluor 647 donkey anti-chicken IgG (H + L) (1:500, ab150175, Abam). DAPI was used to stain cellular nuclei (1:1000, ab104139, Abcam). Immunoreactivity was analyzed by NIH ImageJ software.

Real-time quantitative PCR

Total RNA was isolated from the hippocampus using TRIzol Reagent (Invitrogen). Subsequently, reverse transcribed (1 μg RNA per reaction) into complementary DNA using the HiScript II Q Select RT SuperMix for qPCR (+ gDNA wiper) (R233-01, Vazyme, Nanjing, China). qPCR was performed using the ChamQ SYBR qPCR Master Mix (High ROX Premixed) (Q341-02, Vazyme) and the primers listed in supplemental information Table S2, on a real-time PCR system. Expression levels were calculated using the $2^{-\Delta\Delta Cq}$ method and normalized to GAPDH expression.

Western blot analysis

After behavioral tests, hippocampal tissues were harvested under terminal anesthesia and the equivalent amounts of protein in different groups were separated by 10% SDS-PAGE and transferred onto a polyvinylidene fluoride membrane (Millipore). The membranes were sequentially incubated with anti-ITSN1 antibody (Proteintech, cat no. 21862-1-AP, Rabbit, 1:2000), anti-JNK antibody (Proteintech, cat no. 66210-1-Ig, Mouse, 1:3000), anti-p-JNK antibody (Abcam, cat no. ab124956, Rabbit, 1:3000), anti-JUN antibody (Proteintech, cat no. 66313-1-Ig, Mouse, 1:5000), anti-p-c-JUN antibody (Proteintech, cat no. 28891-1-AP, Rabbit, 1:1000), anti-PSD95 antibody (Proteintech, cat no. 20665-1-AP, Rabbit, 1:5000), anti-synaptophysin antibody (HUABIO, cat no. ET1606-56, Rabbit, 1:5,000), anti-EIF4A3 antibody (Proteintech, cat no. 17504-1-AP, Rabbit, 1:2000), anti-α-tubulin antibody (Proteintech, cat no. 80762-1-RR, Rabbit, 1:5000), and anti-GAPDH antibody (Proteintech, cat no. 60004-1-Ig, Mouse, 1:15000) overnight at 4°C. Membranes were incubated with secondary antibodies, including goat anti-rabbit IgG antibody (Cell Signaling Technology, cat no. 7074P2, 1:3000) and goat anti-mouse IgG antibody (Proteintech, cat no. RGAM001, 1:3000). Immunoreactivity was detected with enhanced chemiluminescence fluorescent detection reagent and analyzed by NIH ImageJ software. GAPDH or α-tubulin was used as a loading control.

Generation of stable circITSN1 overexpressing HT-22 cells

To achieve lentivirus-mediated circITSN1 overexpression, the lentivirus vectors pcSLenti and pcSLenti harboring circITSN1 (pcSLenti-EF1-EGFP-F2A-Puro-CMV-S-circITSN1) were purchased from OBiO Technology (Shanghai, China). Then, pcSLenti and pcSLenti-EF1-EGFP-F2A-Puro-CMV-S-circITSN1 were used to transfect HT22 cells independently at an MOI of 10. HT22 cells stably expressed circITSN1. RT-qPCR was used to test the expression of circITSN1.

EIF4A3 small interfering RNA (siRNA)

Upon reaching 50%–60% confluence, HT22 cells were transfected with specific siRNA (OBiO Technology, Shanghai, China) or negative control siRNA (OBiO Technology, Shanghai, China) using Lipofectamine 3000 (Thermo Fisher Scientific, Waltham, MA, USA) in Opti-MEM (Gibco, Thermo Fisher Scientific, Waltham, MA, USA); EIF4A3 siRNA target sequence, sense strand 5′- CGUGCUAUCA AGCAGAUAAUUTT-3′, antisense strand 5′- AAUUAUCUGCUU GAUAGCACGTT-3′. After 8 h of transfection, the medium was replaced with Dulbecco's modified Eagle medium (DMEM), and the cells were cultured for an additional 48 h.

Actinomycin D assay

Actinomycin D can inhibit RNA polymerase activity and prevent new mRNA synthesis. HT-22 cells, a mouse hippocampal neuronal cell line, were treated with 2 mg/mL actinomycin D (Merck, Germany) to block transcription. Then, the remaining RNAs extracted from treated cells were assessed with RTqPCR.

Statistical analysis

Data are presented as the mean ± SD, medians (quartiles), or proportions where appropriate. The normality was tested with the Shapiro-Wilks test. Two-group comparisons were analyzed using an unpaired Student's t test. One-way or two-way ANOVA followed by a post hoc test was used for multiple comparisons in GraphPad Prism 8 (GraphPad Software, CA, USA). Probability values less than 0.05 ($p < 0.05$) were considered statistically significant. $^{*}p < 0.05$, $^{**}p < 0.01$, $^{***}p < 0.0001$, and $^{****}p < 0.0001$.

DATA AVAILABILITY

The data are available from corresponding author on reasonable request.

ACKNOWLEDGMENTS

This study was supported by the National Natural Science Foundation of China (grant no. 81870858 to C.C.), the National Natural Science Foundation of China (grant no. 82201426 to R.G.), and the Natural Science Foundation of Sichuan Province (grant no. 2024NSFSC1644 to X. Zeng).

AUTHOR CONTRIBUTIONS

C.Z. and X. Zhu, conceptualization, methodology, software, validation, formal analysis, investigation, data curation, and writing – original draft. C.C., validation, conceptualization, methodology, software, writing—review and editing, visualization, supervision, project administration, and funding acquisition. R.G., H.C., H.Y., W.L.,C.Y., L.Y., and X. Zeng, investigation, writing – review and editing, and resources. T.Z., D.M., J.L., and Q.L., writing – reviewing and editing, supervision, project administration, and funding acquisition.

DECLARATION OF INTERESTS

The authors declare no competing interests.

SUPPLEMENTAL INFORMATION

Supplemental information can be found online at https://doi.org/10.1016/j.omtn.2025.102555.

REFERENCES

1. Bhushan, S., Li, Y., Huang, X., Cheng, H., Gao, K., and Xiao, Z. (2021). Progress of research in postoperative cognitive dysfunction in cardiac surgery patients: A review article. Int. J. Surg. *95*, 106163.
2. Peng, W., Lu, W., Jiang, X., Xiong, C., Chai, H., Cai, L., and Lan, Z. (2023). Current Progress on Neuroinflammation-mediated Postoperative Cognitive Dysfunction: An Update. Curr. Mol. Med. *23*, 1077–1086.
3. Boone, M.D., Sites, B., von Recklinghausen, F.M., Mueller, A., Taenzer, A.H., and Shaefi, S. (2020). Economic Burden of Postoperative Neurocognitive Disorders Among US Medicare Patients. JAMA Netw. Open *3*, e208931.
4. Thedim, M., and Vacas, S. (2025). Anesthetic sensitivity and resilience in the aging brain: implications for perioperative neurocognitive disorders. Anesthesiol. Perioper. Sci. *3*, 11.
5. Wang, P., Velagapudi, R., Kong, C., Rodriguiz, R.M., Wetsel, W.C., Yang, T., Berger, M., Gelbard, H.A., Colton, C.A., and Terrando, N. (2020). Neurovascular and immune mechanisms that regulate postoperative delirium superimposed on dementia. Alzheimer's Dement. *16*, 734–749.
6. Vacas, S., Cole, D.J., and Cannesson, M. (2021). Cognitive Decline Associated With Anesthesia and Surgery in Older Patients. JAMA *326*, 863–864.
7. Serna-Rodríguez, M.F., Bernal-Vega, S., de la Barquera, J.A.O.S., Camacho-Morales, A., and Pérez-Maya, A.A. (2022). The role of damage associated molecular pattern molecules (DAMPs) and permeability of the blood-brain barrier in depression and neuroinflammation. J. Neuroimmunol. *371*, 577951.
8. Margraf, A., Ludwig, N., Zarbock, A., and Rossaint, J. (2020). Systemic Inflammatory Response Syndrome After Surgery: Mechanisms and Protection. Anesth. Analg. *131*, 1693–1707.
9. Tang, X., Li, J., Yang, B., Lei, C., and Dong, H. (2023). Efficacy of sleep interventions on postoperative delirium: a systematic review and meta-analysis of randomized controlled trials. Anesthesiol. Perioper. Sci. *1*, 29.
10. Piscopo, P., Manzini, V., Rivabene, R., Crestini, A., Le Pera, L., Pizzi, E., Veroni, C., Talarico, G., Peconi, M., Castellano, A.E., et al. (2022). A Plasma Circular RNA Profile Differentiates Subjects with Alzheimer's Disease and Mild Cognitive Impairment from Healthy Controls. Int. J. Mol. Sci. *23*, 13232.
11. Yang, Y.S., He, S.L., Chen, W.C., Wang, C.M., Huang, Q.M., Shi, Y.C., Lin, S., and He, H.F. (2022). Recent progress on the role of non-coding RNA in postoperative cognitive dysfunction. Front. Cell. Neurosci. *16*, 1024475.
12. Najafi, S., Aghaei Zarch, S.M., Majidpoor, J., Pordel, S., Aghamiri, S., Fatih Rasul, M., Asemani, Y., Vakili, O., Mohammadi, V., Movahedpour, A., and Arghiani, N. (2023). Recent insights into the roles of circular RNAs in human brain development and neurologic diseases. Int. J. Biol. Macromol. *225*, 1038–1048.
13. Wu, D.P., Zhao, Y.D., Yan, Q.Q., Liu, L.L., Wei, Y.S., and Huang, J.L. (2023). Circular RNAs: emerging players in brain aging and neurodegenerative diseases. J. Pathol. *259*, 1–9.
14. Wen, G., Zhou, T., and Gu, W. (2021). The potential of using blood circular RNA as liquid biopsy biomarker for human diseases. Protein Cell *12*, 911–946.
15. Wen, G., and Gu, W. (2022). Circular RNAs in peripheral blood mononuclear cells are more stable than linear RNAs upon sample processing delay. J. Cell Mol. Med. *26*, 5021–5032.
16. Zhang, M.X., Lin, J.R., Yang, S.T., Zou, J., Xue, Y., Feng, C.Z., and Cao, L. (2022). Characterization of circRNA-Associated-ceRNA Networks Involved in the Pathogenesis of Postoperative Cognitive Dysfunction in Aging Mice. Front. Aging Neurosci. *14*, 727805.
17. Tang, J., Tang, Y., Lin, P., Zheng, J., Li, Z., and Zhang, Y. (2024). Integrative analysis of circRNA networks in postoperative cognitive dysfunction. Int. J. Neurosci. *135*, 455–487.
18. Ran, W., Liang, N., Yuan, R., Wang, Z., and Gao, J. (2022). Identification of Potential Key circRNAs in Aged Mice With Postoperative Delirium. Front. Mol. Neurosci. *15*, 836534.
19. Komulainen, E., Varidaki, A., Kulesskaya, N., Mohammad, H., Sourander, C., Rauvala, H., and Coffey, E.T. (2020). Impact of JNK and Its Substrates on Dendritic Spine Morphology. Cells *9*, 440.
20. Singh, A., Upadhayay, S., and Mehan, S. (2021). Understanding Abnormal c-JNK/p38MAPK Signaling Overactivation Involved in the Progression of Multiple Sclerosis: Possible Therapeutic Targets and Impact on Neurodegenerative Diseases. Neurotox. Res. *39*, 1630–1650.
21. Yang, Z., Xie, L., Han, L., Qu, X., Yang, Y., Zhang, Y., He, Z., Wang, Y., and Li, J. (2017). Circular RNAs: Regulators of Cancer-Related Signaling Pathways and Potential Diagnostic Biomarkers for Human Cancers. Theranostics *7*, 3106–3117.
22. Malakooti, N., Pritchard, M.A., Chen, F., Yu, Y., Sgambelloni, C., Adlard, P.A., and Finkelstein, D.I. (2020). The Long Isoform of Intersectin-1 Has a Role in Learning and Memory. Front. Behav. Neurosci. *14*, 24.
23. Zhu, F., Luo, E., Yi, F., Xiong, J., Huang, C., and Li, R. (2021). LncRNA ITSN1-2 knockdown inhibits OGD/R-induced inflammation and apoptosis in mouse hippocampal neurons via sponging miR-195-5p. Neuroreport *32*, 1325–1334.
24. Wang, X., Chen, M., and Fang, L. (2021). hsa_circ_0068631 promotes breast cancer progression through c-Myc by binding to EIF4A3. Mol. Ther. Nucleic Acids *26*, 122–134.
25. Wong, R., Zhang, Y., Zhao, H., and Ma, D. (2022). Circular RNAs in organ injury: recent development. J. Transl. Med. *20*, 533.

26. Li, J., Sun, C., Cui, H., Sun, J., and Zhou, P. (2021). Role of circRNAs in neurodevelopment and neurodegenerative diseases. J. Mol. Neurosci. *71*, 1743–1751.

27. Wu, Y.Q., Liu, Q., Wang, H.B., Chen, C., Huang, H., Sun, Y.M., Ma, L.H., Wan, J., Sun, Y.Y., and Miao, H.H. (2021). Microarray Analysis Identifies Key Differentially Expressed Circular RNAs in Aged Mice With Postoperative Cognitive Dysfunction. Front. Aging Neurosci. *13*, 716383.

28. Gao, R., Chen, C., Zhao, Q., Li, M., Wang, Q., Zhou, L., Chen, E., Chen, H., Zhang, Y., Cai, X., et al. (2020). Identification of the Potential Key Circular RNAs in Elderly Patients With Postoperative Cognitive Dysfunction. Front. Aging Neurosci. *12*, 165.

29. Jakob, B., Kochlamazashvili, G., Jäpel, M., Gauhar, A., Bock, H.H., Maritzen, T., and Haucke, V. (2017). Intersectin 1 is a component of the Reelin pathway to regulate neuronal migration and synaptic plasticity in the hippocampus. Proc. Natl. Acad. Sci. USA *114*, 5533–5538.

30. Mehta, S.L., Dempsey, R.J., and Vemuganti, R. (2020). Role of circular RNAs in brain development and CNS diseases. Prog. Neurobiol. *186*, 101746.

31. Misir, S., Wu, N., and Yang, B.B. (2022). Specific expression and functions of circular RNAs. Cell Death Differ. *29*, 481–491.

32. Qian, X., Zheng, S., and Yu, Y. (2022). CircUBE3B High Expression Participates in Sevoflurane-Induced Human Hippocampal Neuron Injury via Targeting miR-326 and Regulating MYD88 Expression. Neurotox. Res. *41*, 16–28.

33. Song, C., Zhang, Y., Huang, W., Shi, J., Huang, Q., Jiang, M., Qiu, Y., Wang, T., Chen, H., and Wang, H. (2022). Circular RNA Cwc27 contributes to Alzheimer's disease pathogenesis by repressing Pur-α activity. Cell Death Differ. *29*, 393–406.

34. Ye, J., She, X., Liu, Z., He, Z., Gao, X., Lu, L., Liang, R., and Lin, Y. (2021). Eukaryotic Initiation Factor 4A-3: A Review of Its Physiological Role and Involvement in Oncogenesis. Front. Oncol. *11*, 712045.

35. Viphakone, N., Sudbery, I., Griffith, L., Heath, C.G., Sims, D., and Wilson, S.A. (2019). Co-transcriptional Loading of RNA Export Factors Shapes the Human Transcriptome. Mol. Cell *75*, 310–323.e8.

36. Song, H., Liu, Y., Li, X., Chen, S., Xie, R., Chen, D., Gao, H., Wang, G., Cai, B., and Yang, X. (2020). Long noncoding RNA CASC11 promotes hepatocarcinogenesis and HCC progression through EIF4A3-mediated E2F1 activation. Clin. Transl. Med. *10*, e220.

37. Yang, Y.M., Fekete, A., Arsenault, J., Sengar, A.S., Aitoubah, J., Grande, G., Li, A., Salter, E.W., Wang, A., Mark, M.D., et al. (2024). Intersectin-1 enhances calcium-dependent replenishment of the readily releasable pool of synaptic vesicles during development. J. Physiol. https://doi.org/10.1113/JP286462.

38. Mintoo, M., Rajagopalan, V., and O'Bryan, J.P. (2024). Intersectin - many facets of a scaffold protein. Biochem. Soc. Trans. *52*, 1–13.

39. Kraus, M., Pleskot, R., and Van Damme, D. (2024). Structural and Evolutionary Aspects of Plant Endocytosis. Annu. Rev. Plant Biol. *75*, 521–550.

40. Jaye, S., Sandau, U.S., McFarland, T.J., Woltjer, R.L., and Saugstad, J.A. (2024). A clathrin mediated endocytosis scaffolding protein, Intersectin 1, changes in an isoform, brain region, and sex specific manner in Alzheimer's disease. Front. Neurosci. *18*, 1426180.

41. Skuladottir, A.T., Tragante, V., Sveinbjornsson, G., Helgason, H., Sturluson, A., Bjornsdottir, A., Jonsson, P., Palmadottir, V., Sveinsson, O.A., Jensson, B.O., et al. (2024). Loss-of-function variants in ITSN1 confer high risk of Parkinson's disease. NPJ Parkinsons Dis. *10*, 140.

42. Li, D., Chen, M., Meng, T., and Fei, J. (2020). Hippocampal microglial activation triggers a neurotoxic-specific astrocyte response and mediates etomidate-induced long-term synaptic inhibition. J. Neuroinflammation *17*, 109.

43. Min, J., Lai, Z., Wang, H., and Zuo, Z. (2022). Preoperative environment enrichment preserved neuroligin 1 expression possibly via epigenetic regulation to reduce postoperative cognitive dysfunction in mice. CNS Neurosci. Ther. *28*, 619–629.

44. Zhao, Y., Kuca, K., Wu, W., Wang, X., Nepovimova, E., Musilek, K., and Wu, Q. (2022). Hypothesis: JNK signaling is a therapeutic target of neurodegenerative diseases. Alzheimer's Dement. *18*, 152–158.

45. Castro-Torres, R.D., Olloquequi, J., Parcerisas, A., Ureña, J., Ettcheto, M., Beas-Zarate, C., Camins, A., Verdaguer, E., and Auladell, C. (2024). JNK signaling and its impact on neural cell maturation and differentiation. Life Sci. *350*, 122750.

46. Shi, Z., Zhang, K., Zhou, H., Jiang, L., Xie, B., Wang, R., Xia, W., Yin, Y., Gao, Z., Cui, D., et al. (2020). Increased miR-34c mediates synaptic deficits by targeting synaptotagmin 1 through ROS-JNK-p53 pathway in Alzheimer's Disease. Aging Cell *19*, e13125.

47. Zhang, L.Q., Gao, S.J., Sun, J., Li, D.Y., Wu, J.Y., Song, F.H., Liu, D.Q., Zhou, Y.Q., and Mei, W. (2022). DKK3 ameliorates neuropathic pain via inhibiting ASK-1/JNK/p-38-mediated microglia polarization and neuroinflammation. J. Neuroinflammation *19*, 129.

48. Morel, C., Sherrin, T., Kennedy, N.J., Forest, K.H., Avcioglu Barutcu, S., Robles, M., Carpenter-Hyland, E., Alfulaij, N., Standen, C.L., Nichols, R.A., et al. (2018). JIP1-Mediated JNK Activation Negatively Regulates Synaptic Plasticity and Spatial Memory. J. Neurosci. *38*, 3708–3728.

49. Lin, H., Kang, Z., Li, S., Zeng, J., and Zhao, J. (2022). Sarm1 is Essential for Anesthesia-Induced Neuroinflammation and Cognitive Impairment in Aged Mice. Cell. Mol. Neurobiol. *42*, 1465–1476.

50. Rossato, J.I., Radiske, A., Gonzalez, M.C., Bevilaqua, L.R.M., and Cammarota, M. (2022). On the effect of hippocampal c-Jun N-terminal kinase inhibition on object recognition memory. Front. Behav. Neurosci. *16*, 1052124.

51. Hammouda, M.B., Ford, A.E., Liu, Y., and Zhang, J.Y. (2020). The JNK Signaling Pathway in Inflammatory Skin Disorders and Cancer. Cells *9*, 857.

52. He, A.T., Liu, J., Li, F., and Yang, B.B. (2021). Targeting circular RNAs as a therapeutic approach: current strategies and challenges. Signal Transduct. Target. Ther. *6*, 185.

53. Kilkenny, C., Browne, W.J., Cuthill, I.C., Emerson, M., and Altman, D.G. (2010). Improving bioscience research reporting: the ARRIVE guidelines for reporting animal research. PLoS Biol. *8*, e1000412.

54. Vizcaychipi, M.P., Watts, H.R., O'Dea, K.P., Lloyd, D.G., Penn, J.W., Wan, Y., Pac-Soo, C., Takata, M., and Ma, D. (2014). The therapeutic potential of atorvastatin in a mouse model of postoperative cognitive decline. Ann. Surg. *259*, 1235–1244.